

Perturbative model for the second-order velocity structure function tensor in turbulent shear flows

Samvit Kumar¹, Charles Meneveau¹, and Gregory Eyink^{1,2}

¹*Department of Mechanical Engineering, Johns Hopkins University, Baltimore, Maryland 21218, USA*

²*Department of Applied Mathematics, Johns Hopkins University, Baltimore, Maryland 21218, USA*



(Received 6 January 2022; accepted 23 May 2022; published 14 June 2022)

A model for the structure function tensor is proposed, incorporating the effect of anisotropy as a linear perturbation to the standard isotropic form. The analysis extends the spectral approach of Ishihara *et al.* [T. Ishihara, *Phys. Rev. Lett.* **88**, 154501 (2002)] to physical space based on Kolmogorov's theory and is valid in the inertial range of turbulence. Previous results for velocity cospectra are used to obtain estimates of the model coefficients. Structure functions measured from direct numerical simulations of channel flow and from experimental measurements in turbulent boundary layers are compared with predicted behavior and reasonable agreement is found. We note that power-law scaling is more evident in the cospectra than for the mixed structure functions. Observations are made about countergradient correlation between Fourier modes of wall-normal and streamwise velocity components for wave numbers approaching the Kolmogorov scale.

DOI: [10.1103/PhysRevFluids.7.064601](https://doi.org/10.1103/PhysRevFluids.7.064601)

I. INTRODUCTION

The second-order two-point structure function is one of the most fundamental statistical characterizations of a turbulent velocity field. It is defined to be the covariance of the velocity difference between two points \mathbf{x} and $\mathbf{x} + \mathbf{r}$,

$$D_{ij}(\mathbf{r}) = \langle [u_i(\mathbf{x} + \mathbf{r}) - u_i(\mathbf{x})][u_j(\mathbf{x} + \mathbf{r}) - u_j(\mathbf{x})] \rangle, \quad (1)$$

where $\langle \cdot \rangle$ denotes averaging (e.g., over time, realizations, or a region in space). The statistics of the small scales of turbulence (i.e., for $r = |\mathbf{r}|$ much smaller than the size of the large-scale eddies in a turbulent flow) are widely accepted to approach isotropic behavior in the limit of very large Reynolds number [1,2]. This is reflected in the simple inertial range isotropic model of the structure function tensor [1]. Specifically, under the assumption of local isotropy for a divergence-free turbulent velocity field and according to the 1941 version of the Kolmogorov theory (K41) neglecting effects of intermittency [1,2], the structure function tensor can be expressed as

$$D_{ij}^{(0)}(\mathbf{r}) = C_0(\epsilon r)^{2/3} \left(\frac{4}{3} \delta_{ij} - \frac{1}{3} \frac{r_i r_j}{r^2} \right), \quad (2)$$

where ϵ is the mean turbulent kinetic energy dissipation and C_0 is a constant. The special case of the inertial-range scaling of the streamwise longitudinal structure function $D_{11}(r\mathbf{e}_1)$, where \mathbf{e}_1 is the streamwise unit vector, has been studied extensively in a variety of turbulent flows [3–9].

Focusing on displacements covering both the so-called production and the inertial ranges, i.e., for both $r > y$ and $\eta < r < y$ (where y is the distance to the wall, i.e., indicative of the local integral scale of motion, and η is the Kolmogorov scale), the longitudinal structure function in high-Reynolds-number turbulent wall-bounded flow experiments was studied by de Silva *et al.* [10]. The study also reported on scaling properties of higher-order longitudinal structure functions,

identifying logarithmic scaling in the production range and power-law scaling in the inertial range for all moment orders.

The structure and scaling of $D_{ij}(\mathbf{r})$ for other combinations of indices i and j have been examined recently [11] in the context of the attached eddy hypothesis and the random additive process model, for wall-parallel displacements r in the production range $r > y$. For the wall-parallel velocity components, logarithmic behavior could again be obtained, while the mixed structure function D_{12} in the production range $r > y$ tends to a constant equal to twice the turbulent shear stress (i.e., $D_{12} \rightarrow -2\langle u'_1 u'_2 \rangle$, where \mathbf{e}_1 and \mathbf{e}_2 denote the mean-flow streamwise and wall-normal directions, respectively). At smaller scales $r < y$, the mixed structure function $D_{12}^{(0)}(r\mathbf{e}_1)$ with displacements in the horizontal plane is, according to Eq. (2), exactly zero. The following question thus arises: How does the mixed structure function, or more generally the entire tensor object $D_{ij}(\mathbf{r})$, go from its constant value (or logarithmic trends) in the production range to zero at small scales? Such considerations require a description of large-scale shear effects on the structure of turbulence.

In order to include the effects of shear, we propose a structure function model following the methodology applied by Ishihara *et al.* [12] in the context of a spectral model and by Kaneda [13] to velocity correlations. It is based on three assumptions [12]. (i) The mean velocity field \mathbf{U} is assumed to have a small spatial mean velocity gradient $S_{mn} = \partial U_m / \partial x_n$. The coupling between the fluctuating field \mathbf{u} and the mean field \mathbf{U} is associated with a timescale $(\tau_S) \sim O(1/|\mathbf{S}|)$. Conversely, according to Kolmogorov theory, the nonlinear coupling within the fluctuating field is associated with a timescale $(\tau_r) \sim O(r^{2/3}/\epsilon^{1/3})$, for eddies of length scale r . This implies that for small enough r , as in the inertial range, the latter interactions are faster and the effect of the mean velocity, while not negligible, is small. (ii) Therefore, it is reasonable to assume that the velocity structure function, with r in the inertial range at high Reynolds numbers, is well approximated by

$$D_{ij}(\mathbf{r}) = D_{ij}^{(0)}(\mathbf{r}) + D_{ij}^{(1)}(\mathbf{r}), \quad (3)$$

where the second term is smaller than the first by a ratio of the order of τ_r/τ_S . The term $D_{ij}^{(1)}(\mathbf{r})$ accounts for the mean velocity gradient and acts as an anisotropic perturbation or correction to the isotropic part. (iii) We also assume that for small τ_r/τ_S , $D_{ij}^{(1)}(\mathbf{r})$ is linear in \mathbf{S} . Taken together and following the arguments in [12], it follows that there exists a fourth-rank tensor C_{ijmn} such that

$$D_{ij}^{(1)}(\mathbf{r}) = C_{ijmn}(\mathbf{r}) S_{mn}, \quad (4)$$

where S_{mn} is the mean velocity gradient tensor and $C_{ijmn}(\mathbf{r})$ is an isotropic fourth-rank tensor function of the vector \mathbf{r} .

The main objective of this work is to extend the work of Ishihara *et al.* [12] to physical space and determine the corresponding second-order structure function tensor $D_{ij}(\mathbf{r})$ by formulating the appropriate form of the fourth-rank tensor $C_{ijmn}(\mathbf{r})$. A review of prior work is presented in Sec. II, followed by the main derivations in Sec. III. To compare the model predictions with data, we use channel flow DNS turbulence data at two Reynolds numbers accessed from the Johns Hopkins Turbulence Database [14–16]. We compute the structure functions and spectra in the logarithmic layer and compare their behavior for the inertial subrange with the proposed model in Sec. IV. Structure function measurements for the atmospheric boundary layer from Kurien and Sreenivasan [17] are also included, as are experimental results for a turbulent boundary layer from Jacob *et al.* [9] and structure function measurements from Yang *et al.* [11] (based on analysis of the experimental data described by Talluru *et al.* [18]). We confirm that the data trends towards predicted theoretical behavior for the moderate-Reynolds-number channel flow results, while the experimental measurements at much higher Reynolds numbers show wider scaling ranges, as expected. Conclusions are summarized in Sec. V.

II. PRIOR WORK

Several approaches have previously been proposed for incorporating effects of large-scale shear and anisotropy [4,8] on structure functions. The pioneering work of Arad *et al.* [7] has brought about significant developments in using group theory (SO3) and expansions into spherical harmonics (see Ref. [8] for a detailed review). The effects of intermittency were also included there and are of particular relevance to structure functions of higher order. Even though the general mathematical theory has been largely developed, a full determination of the tensor that also includes the calculation of prefactors, and special cases such as the mixed structure function involving two different velocity components, remains to be carried out. In the present work we focus on second-order structure functions in the inertial range, where prior works, such as the experimental study of Kurien *et al.* [19], suggest that the departure from Kolmogorov (K41) phenomenological theory [20,21] behavior is small. It is possible to extend the present work while incorporating intermittency effects, but at present we operate under the purview of the K41 theory [20,21], neglecting intermittency in order to fully determine the structure function tensor in the inertial range. For the finite Reynolds numbers considered, the theory will only be valid for a small range of length scales. Further refinements on the present approach, left for future work, could include incorporation of intermittency and finite-Reynolds-number corrections.

We follow especially the work of Ishihara *et al.* [12], which developed a model of the spectral tensor based on a linear tensorial perturbation to the isotropic model for a given mean velocity gradient. The velocity correlation tensor $B_{ij}(\mathbf{r}) = \langle u_i(\mathbf{x})u_j(\mathbf{x} + \mathbf{r}) \rangle$ and the structure function tensor are related by

$$D_{ij}(\mathbf{r}) = 2[B_{ij}(\mathbf{0}) - B_{ij}(\mathbf{r})]. \quad (5)$$

This relation enables calculation of the corresponding components of the structure function from the spectrum [5] through a Fourier transform. Specifically, when applied in particular directions (e.g., streamwise for $\mathbf{r} = r\mathbf{e}_1$ or spanwise $\mathbf{r} = r\mathbf{e}_3$) this relation will enable us to use results from previous theoretical and experimental studies [1,3,4,12,22,23] for needed comparisons.

Consider the case of a simple shear flow with mean velocity \mathbf{U} where the mean velocity gradient tensor is given by $S_{ij} = \partial U_i / \partial x_j$ and is assumed to be constant in space (strictly speaking, this condition is not met in wall-bounded turbulence where the shear depends on wall distance). For a shear rate γ , i.e., for $S_{ij} = \gamma \delta_{i1} \delta_{j2}$, a well-known ansatz, due to Lumley [1,4], states that the streamwise shear-stress spectrum $\tilde{E}_{12}(k_1)$ is given by

$$\tilde{E}_{12}(k_1) = -C_1 \gamma \epsilon^{1/3} k_1^{-7/3} \quad \text{for } \gamma^{3/2} \epsilon^{-1/2} \ll k_1 \ll \eta^{-1}, \quad (6)$$

where η is the Kolmogorov length scale. For wall-bounded turbulence in the logarithmic (constant stress) region (where $\gamma = u_\tau / \kappa y$, with u_τ the friction velocity and κ the von Kármán coefficient, and where under the assumption of equality of production and dissipation one has $\epsilon = u_\tau^3 / \kappa y$), we note that the lower-wave-number limit also corresponds to $(\kappa y)^{-1}$. Lumley's result (6) for wave numbers in the inertial range of scales can be used to derive the well-established corresponding result for the inertial range structure function

$$\begin{aligned} D_{12}(r\mathbf{e}_1) &= -2 \int_0^\infty C_1 \gamma \epsilon^{1/3} k_1^{-7/3} [1 - \cos(k_1 r)] dk_1 \\ &= -2C_1 \gamma \epsilon^{1/3} r^{4/3} \int_0^\infty z^{-7/3} (1 - \cos z) dz = -\Gamma\left(-\frac{4}{3}\right) C_1 \gamma \epsilon^{1/3} r^{4/3} \approx -3.047 C_1 \gamma \epsilon^{1/3} r^{4/3}, \end{aligned} \quad (7)$$

where $\Gamma(z)$ is the standard Gamma function. In this way, knowing the value of the coefficient C_1 for the spectrum, we may calculate the mixed structure function in the inertial range as well. An analogous result can also be obtained for the spanwise shear spectrum $\tilde{E}_{12}(k_3)$ and the corresponding spanwise structure function. More in general, however, to connect spectra and structure functions

for all of the structure function tensor's elements in arbitrary directions in the inertial range, we require a description of the full spectral tensor.

For this purpose we recall an important development by Ishihara *et al.* [12], who developed a model for the full spectral tensor in turbulence under the presence of shear. The velocity spectral tensor Q_{ij} is defined as the Fourier transform of the velocity correlation tensor: $Q_{ij}(\mathbf{k}) = (2\pi)^{-3} \int B_{ij}(\mathbf{r}) e^{-i\mathbf{k} \cdot \mathbf{r}} d^3 \mathbf{r}$. They observed that the equations for the fluctuating velocity field are governed by terms which represent (i) the bilinear coupling between the mean velocity field and the mean and fluctuating fields and (ii) the nonlinear coupling within the fluctuating field. In the inertial subrange, Kolmogorov's phenomenological theory is used to show that the latter nonlinear term dominates. Therefore, the effect of mean shear is incorporated as a linear perturbation to the isotropic spectrum as follows:

$$Q_{ij}(\mathbf{k}) = Q_{ij}^{(0)}(\mathbf{k}) + Q_{ij}^{(1)}(\mathbf{k}). \quad (8)$$

Here $Q_{ij}^{(0)}$ is the isotropic Kolmogorov spectrum and $Q_{ij}^{(1)}$ represents the mean shear effect for wave numbers in the inertial range. The two terms are modeled as

$$Q_{ij}^{(0)}(\mathbf{k}) = \frac{K_0}{4\pi} \epsilon^{2/3} k^{-11/3} \left(\delta_{ij} - \frac{k_i k_j}{k^2} \right) = \frac{K_0}{4\pi} \epsilon^{2/3} k^{-11/3} P_{ij}(\mathbf{k}), \quad (9)$$

$$Q_{ij}^{(1)}(\mathbf{k}) = G_{ij\alpha\beta}(\mathbf{k}) S_{\alpha\beta}, \quad (10)$$

where $P_{ij}(\mathbf{k})$ is the projection tensor. The fourth-rank tensor $G_{ij\alpha\beta}$ is determined by applying the divergence-free condition and utilizing symmetry properties. Without loss of generality, we may then write [12]

$$G_{ij\alpha\beta}(\mathbf{k}) = a(k) [P_{i\alpha}(\mathbf{k}) P_{j\beta}(\mathbf{k}) + P_{i\beta}(\mathbf{k}) P_{j\alpha}(\mathbf{k})] + b(k) P_{ij}(\mathbf{k}) \frac{k_\alpha k_\beta}{k^2} \quad (11)$$

for any traceless tensor $S_{\alpha\beta}$. According to the Kolmogorov theory in the inertial range, the tensor $G_{ij\alpha\beta}$ can only depend on ϵ and \mathbf{k} . Dimensional analysis is applied to obtain the functions $a(k) = A\epsilon^{1/3} k^{-13/3}$ and $b(k) = B\epsilon^{1/3} k^{-13/3}$, where A and B are taken to be universal constants. Based on direct numerical simulations (DNSs) of homogeneous shear flow, Ishihara *et al.* [12] determined the numerical values of these parameters as $A = -0.16 \pm 0.03$ and $B = -0.40 \pm 0.06$.

III. CONSTRUCTION OF THE TENSOR C_{ijmn}

The fourth-order tensor C_{ijmn} is constructed as a function of the vector \mathbf{r} and the dissipation ϵ , independent of the mean velocity gradient S_{mn} because r is assumed to be in the inertial range and (as discussed above) the perturbation is assumed to scale linearly with the mean velocity gradient. Since it is invariant under rotation of the coordinate system and should be symmetric in the indices (i, j) , without loss of generality C_{ijmn} can be written as

$$\begin{aligned} C_{ijmn}(\mathbf{r}) = & [\delta_{im} \delta_{jn} + \delta_{in} \delta_{jm}] A_1(r) + \frac{r_m r_n}{r^2} \delta_{ij} A_2(r) + \frac{r_i r_j r_m r_n}{r^4} A_3(r) \\ & + \left[\frac{r_i r_m}{r^2} \delta_{jn} + \frac{r_j r_m}{r^2} \delta_{in} \right] A_4(r) + \left[\frac{r_i r_n}{r^2} \delta_{jm} + \frac{r_j r_n}{r^2} \delta_{im} \right] A_5(r). \end{aligned} \quad (12)$$

Here $\{A_1(r), \dots, A_5(r)\}$ are scalar functions of $r = |\mathbf{r}|$ and for r in the inertial range, these scalar functions can also depend on ϵ . Note that a $\delta_{ij} \delta_{mn}$ term is not needed since it would lead to a term proportional to S_{mm} which is zero for divergence-free mean velocity. We know that D_{ij} and $D_{ij}^{(0)}$ are divergence-free; hence $D_{ij}^{(1)}$ must satisfy these properties as well. The application of these conditions to the aforementioned expression results in the following set of equations:

$$\frac{\partial}{\partial r} (A_2 + A_3 + A_4 + A_5) + \frac{2}{r} (A_3 - A_2 - A_4 - A_5) = 0, \quad (13)$$

$$\frac{\partial}{\partial r}(A_1 + A_4) + \frac{1}{r}(A_2 + 3A_4) = 0, \quad (14)$$

$$\frac{\partial}{\partial r}(A_1 + A_5) + \frac{1}{r}(A_2 + 3A_5) = 0. \quad (15)$$

Since the number of unknowns is greater than the number of equations, we need to specify two of the functions. We use K41 theory and state that since r is in the inertial range, the functions $A_1(r)$ and $A_2(r)$ are dependent only on inertial range variables ϵ and r as the anisotropy effect has been incorporated already. Note that since we assume that the effect of the applied shear enters linearly in the shear, dimensional analysis and symmetries leave us no choice but to express the A 's in terms of dissipation ϵ and displacement magnitude r only. There are no further variables to be employed. Mirroring Ishihara *et al.* [12], we thus employ dimensional analysis to write

$$A_1(r) = \alpha\epsilon^{1/3}r^{4/3}, \quad A_2(r) = \beta\epsilon^{1/3}r^{4/3}. \quad (16)$$

The dimensionless constants α and β are determined in the following section. Utilizing the property that $D_{ij}(\mathbf{0}) = 0$, in conjunction with the expressions for A_1 and A_2 and substituting into Eq. (13), we obtain

$$A_3(r) = -\frac{8\alpha - 7\beta}{65}\epsilon^{1/3}r^{4/3}, \quad A_4(r) = A_5(r) = -\frac{4\alpha + 3\beta}{13}\epsilon^{1/3}r^{4/3}. \quad (17)$$

Observe that A_3 , A_4 , and A_5 have the same functional form as A_1 and A_2 , differing only in the dimensionless constants. Finally, the full anisotropic correction is calculated using these functions as

$$D_{ij}^{(1)}(\mathbf{r}) = \left\{ \alpha(\delta_{im}\delta_{jn} + \delta_{in}\delta_{jm}) + \beta\frac{r_m r_n}{r^2}\delta_{ij} - \left(\frac{8\alpha - 7\beta}{65}\right)\frac{r_i r_j r_m r_n}{r^4} - \left(\frac{4\alpha + 3\beta}{13}\right)\left(\frac{r_i r_m}{r^2}\delta_{jn} + \frac{r_j r_m}{r^2}\delta_{in} + \frac{r_i r_n}{r^2}\delta_{jm} + \frac{r_j r_n}{r^2}\delta_{im}\right) \right\} S_{mn}\epsilon^{1/3}r^{4/3}. \quad (18)$$

This form, derived from assumptions (i)–(iii), results in the dependence of $D_{ij}^{(1)}(\mathbf{r})$ on $r^{4/3}$, which is in agreement with known previous analytical and experimental results, including that of Lumley [4] [Eq. (7)]. Since we are operating with the guidance of K41 theory, we are explicitly able to obtain the power of r , but the associated constants must be determined empirically (in the following section). More general approaches which incorporate the effects of intermittency find that the power of r will be a function of the moment order in a nontrivial fashion [8], but we do not explore the issue of intermittency here and focus only on second-order moments. Next the relation between structure functions and spectra allows us to use known results for the spectral tensor to complete our calculation of the prefactors.

Determining the prefactors

Ishihara *et al.* [12] calculated the full velocity spectral tensor for a uniform shear flow using direct numerical simulations. This case, with a constant velocity gradient, can be considered a canonical example of the type of anisotropy we aim to model. We extend their calculations for uniform shear to obtain the constants α and β and hope that these values offer a degree of universality that extends the validity of the Kolmogorov and Lumley theories to more general settings. Consider again the specialized case of shear flow with $S_{mn} = \gamma\delta_{m1}\delta_{n2}$.

It is useful to calculate $D_{12}^{(1)}$ for two cases, with the displacement \mathbf{r} in the streamwise ($\mathbf{r} = r\mathbf{e}_1$) and spanwise ($\mathbf{r} = r\mathbf{e}_3$) directions resulting in

$$D_{12}(r\mathbf{e}_1) = \frac{9\alpha - 3\beta}{13}\gamma\epsilon^{1/3}r^{4/3}, \quad D_{12}(r\mathbf{e}_3) = \alpha\gamma\epsilon^{1/3}r^{4/3}. \quad (19)$$

The relation between the streamwise shear spectrum $\tilde{E}_{12}(k_1)$ (involving a coefficient C_1) and the corresponding structure function $D_{12}(r\mathbf{e}_1)$ has already been stated in the preceding section [Eq. (7)]. A very similar relation can be derived between the corresponding spanwise quantities, the structure function $D_{12}(r\mathbf{e}_3)$ and the spanwise shear spectrum

$$\tilde{E}_{12}(k_3) = -C_2 \gamma \epsilon^{1/3} k_3^{-7/3}, \quad \gamma^{3/2} \epsilon^{-1/2} \ll k_3 \ll \eta^{-1}. \quad (20)$$

The constants C_1 and C_2 featuring in the spectra can be determined in terms of the model constants A and B from Ishihara *et al.* [12] as¹

$$C_1 = \frac{36\pi}{1729}(-33A + 7B), \quad C_2 = \frac{6\pi}{1729}(-398A + 9B). \quad (21)$$

Given the numerical values of the model constants A and B , we obtain $C_1 = 0.16 \pm 0.07$ and $C_2 = 0.65 \pm 0.13$. These constants can then be used to calculate the corresponding structure functions [as in Eq. (7)], yielding

$$D_{12}(r\mathbf{e}_1) = (-0.49 \pm 0.21)\gamma \epsilon^{1/3} r^{4/3}, \quad D_{12}(r\mathbf{e}_3) = (-2.0 \pm 0.40)\gamma \epsilon^{1/3} r^{4/3}. \quad (22)$$

Comparing Eq. (22) with the expressions (19) (the same expressions also hold for the spanwise direction), we complete our model by calculating the structure function constants

$$\begin{aligned} \alpha &= \Gamma\left(-\frac{4}{3}\right) \frac{6\pi}{1729} (398A - 9B) \approx -2.00 \pm 0.40, \\ \beta &= \Gamma\left(-\frac{4}{3}\right) \frac{6\pi}{1729} (336A + 155B) \approx -3.85 \pm 0.46. \end{aligned} \quad (23)$$

Armed with expressions and constants, we test the behavior of structure functions and spectra on data from DNS and experiments to assess the degree of agreement between measurements and predictions.

IV. SPECTRA AND ANISOTROPIC STRUCTURE FUNCTIONS FROM DNS AND EXPERIMENTS

In the inertial range, the behavior of the diagonal elements of the structure function tensor, i.e., $D_{11}(\mathbf{r})$, $D_{22}(\mathbf{r})$, and $D_{33}(\mathbf{r})$, is dominated by the isotropic contribution ($\sim r^{2/3}$) whereas the anisotropic contribution ($\sim r^{4/3}$) is subdominant. Conversely, the only nonzero contributions to the off-diagonal components $D_{12}(\mathbf{r})$, $D_{13}(\mathbf{r})$, and $D_{23}(\mathbf{r})$ are from the anisotropic term; hence, to investigate the validity of the anisotropic model we choose $D_{12}(\mathbf{r})$ as the subject of our study. The values obtained for the constants in the structure function model in the preceding section have assumed a constant uniform shear flow, but we test them on the pressure-driven channel, an oft-studied shear flow ubiquitous in nature and engineering. Channel flow data at $Re_\tau = 1000$ and 5200, available from the Johns Hopkins Turbulence Database (JHTDB) [14,15], are used to compute the streamwise–wall-normal structure function D_{12} with displacement \mathbf{r} in the streamwise [$D_{12}(r\mathbf{e}_1)$] and spanwise [$D_{12}(r\mathbf{e}_3)$] directions and the corresponding cospectra $\phi_{12}(k_1)$ and $\phi_{12}(k_3)$, with \mathbf{e}_1 , \mathbf{e}_2 , and \mathbf{e}_3 representing the streamwise, wall-normal, and spanwise directions, respectively. We compute the structure functions and spectra at different wall-normal distances y within the logarithmic layer by averaging in time and in the homogeneous direction. In the logarithmic layer, it is reasonable to assume that dissipation balances production [16], and the mean velocity gradient $S_{mn} = \gamma \delta_{m1} \delta_{n2} = (u_\tau / \kappa y) \delta_{m1} \delta_{n2}$. The length scale associated with the shear rate equals the wall-normal distance y , which is also the length scale of energy containing eddies in the logarithmic layer and hence the length scale for our measurements.

¹We note the occurrence of 1729, the famous Ramanujan-Hardy number [24], the smallest natural number which can be written as a sum of two cubes in two ways: $1729 = 10^3 + 9^3 = 12^3 + 1^3$.

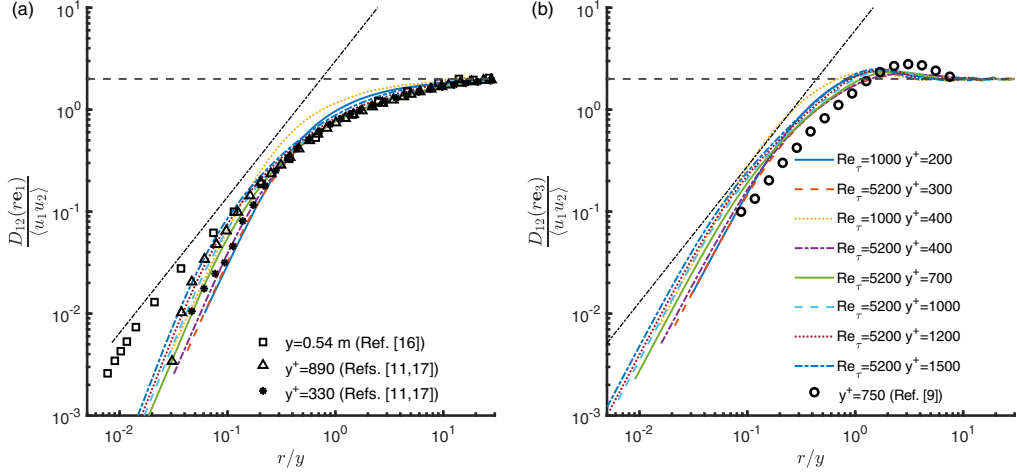


FIG. 1. Structure functions of the streamwise wall-normal velocity in channel flow at $Re_\tau = 1000$ and 5200 from the JHTDB [14–16] at different wall-normal distances $y^+ = yu_\tau/v$, within the logarithmic layer with separation along the (a) streamwise (e_1) and (b) spanwise (e_3) directions. The curves in both plots are described by the legend in (b). Also included in (a) are the atmospheric boundary layer measurements of Kurien and Sreenivasan [17] (□) and the turbulent boundary layer measurements from Baidya and co-workers [11,18] (Δ and $*$) for streamwise separation and in (b) the turbulent boundary layer measurements of Jacob *et al.* [9] for spanwise separation (\circ). The black dot-dashed line in both cases has a slope of $4/3$, representing the predicted inertial range behavior.

Structure function measurements for the atmospheric boundary layer from Kurien and Sreenivasan [17] and for turbulent boundary layers from Jacob *et al.* [9] and Baidya and co-workers [11,18] are compared as well. In all of the comparisons, we use the quoted values of the shear rate (assuming $\gamma = u_\tau/\kappa y$), Reynolds stresses (assuming $\langle u_1 u_2 \rangle = -u_\tau^2$), and $\epsilon = -\gamma \langle u_1 u_2 \rangle = u_\tau^3/\kappa y$ (balance between production and dissipation) at the corresponding y locations. Specifically, for the DNS at $Re_\tau = 1000$, employing the numerical values from the simulation results in $\gamma h/U_b = 121.87/y^+$ and $\epsilon h/U_b^3 = 0.30/y^+$, while at $Re_\tau = 5200$ we obtain $\gamma = 524.75/y^+$ and $\epsilon = 0.90/y^+$. Here U_b represents the bulk velocity and h is the channel half-height (see [15,16]). For the atmospheric data, the dissipation is given as $\epsilon = 1.5 \times 10^{-2} \text{ m}^2 \text{ s}^{-3}$ and assuming $\epsilon = -\gamma \langle u_1 u_2 \rangle$, we have $\gamma = 25.19 \text{ s}^{-1}$. We use the same assumptions for the data set from Baidya and co-workers [11,18] as the DNS data, resulting in $\gamma = 6.1471 \times 10^4/y^+ \text{ s}^{-1}$ and $\epsilon = 2.3630 \times 10^4/y^+ \text{ m}^2 \text{ s}^{-3}$.

Note that our assumptions about the Reynolds stress and production-dissipation balance represent the inertial range behavior and will be accurate for only a small range of y at finite Re . However, since the structure function model itself assumes similar limiting behavior also, consistency is maintained.

The streamwise and spanwise structure functions normalized by the local Reynolds shear stress are plotted in Fig. 1. First, as expected, the plots show that structure functions tend to twice the Reynolds shear stress, as streamwise and spanwise displacements become very large (the results converge for $r > 10y$). The streamwise structure functions monotonically approach the limit, but the spanwise structure functions surpass the limit, reach maxima in magnitude around $r \sim y$, and then decay to the limit. This implies a positive correlation between the two velocity increments, consistent with negative lobes in the spanwise correlation functions and indicating the presence of flow structures having length scales of the order of the wall-normal distance ($\sim y$) for the channel flow as well as the turbulent boundary layer. In the channel flow case, the largest measurable displacement is equal to half the domain size in the corresponding direction, due to periodicity. The smallest separation, on the other hand, is equal to the grid size employed for the simulations.

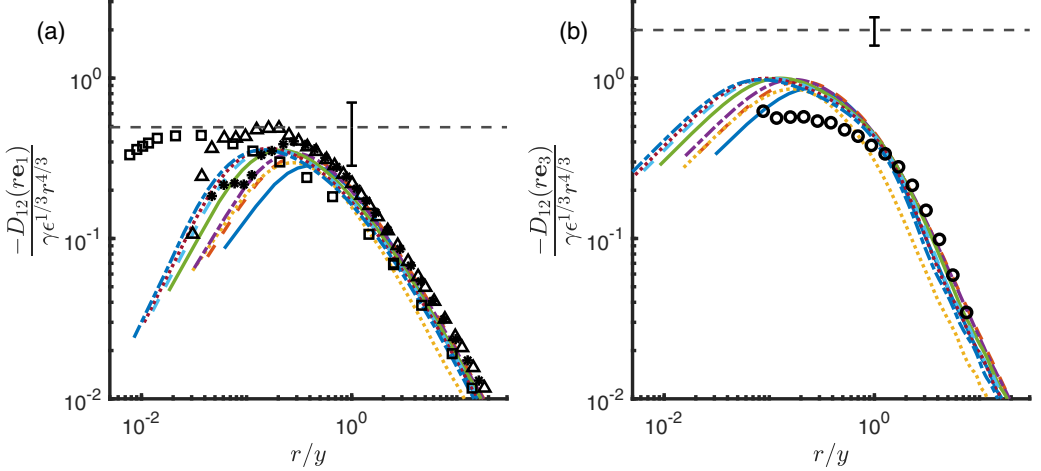


FIG. 2. (a) Compensated streamwise structure functions and (b) compensated spanwise structure functions. Lines and symbols are the same as in Fig. 1. The predicted inertial range behavior is marked by the dashed horizontal lines. The error bars are a result of the uncertainty in the prefactor.

Details of the domain and grid size can be found on the JHTDB website [25] and in Refs. [15,16]. We also plot lines representing the expected 4/3 power law in Fig. 1 and observe that the DNS data at more moderate Reynolds numbers show agreement with such power-law scaling over only a short range of scales [with $0.12 \lesssim r/y \lesssim 0.26$ at $Re_\tau = 5200$ and $y^+ = 1200$ for the streamwise structure function and $0.08 \lesssim r/y \lesssim 0.2$ at $Re_\tau = 5200$ and $y^+ = 700$ for the spanwise structure function being the most extensive ranges of agreement; the range is defined as the scales over which the compensated structure function lies within 5% of the plateau ordinate (discussed in the following paragraph)]. The experimental data display longer power-law scaling.

Next the predictions for the structure function from the anisotropic model are compared with the data by plotting compensated streamwise structure functions $[-D_{12}(r\mathbf{e}_1)/\gamma\epsilon^{1/3}r^{4/3}]$ and compensated spanwise structure functions $[-D_{12}(r\mathbf{e}_3)/\gamma\epsilon^{1/3}r^{4/3}]$ in Figs. 2(a) and 2(b), respectively. The inertial range behavior would imply a plateau in the curve and the ordinate at which it is predicted is marked by a black dashed line, with the error bars representing the computed uncertainty. As the Reynolds number and the distance from the wall increase, so does the separation of scales and the implied extent of the inertial range. As can be seen, the curves from the DNS exhibit a weak trend towards the predicted inertial range behavior and indications of a plateau can be discerned. For streamwise structure functions [Fig. 2(a)], the smallest separation of scales is for the curve at $y^+ = 200$ and $Re_\tau = 1000$, where the inertial range ($\sim r^{4/3}$) behavior is suggested to occur over a small range of scales, producing mostly a crest. As the separation of scales increases, the crest broadens and flattens and also approaches the constant line. This is evident when comparing the curve for $y^+ = 200$ with the curve at $y^+ = 1500$ and $Re_\tau = 5200$. This trend is clearly evident when comparing these curves with the atmospheric boundary layer data from Kurien and Sreenivasan [17], which has significant scale separation with the large scale $y = 0.54$ m and the small scale at $\eta = 0.7$ mm, allowing for a longer inertial range and consequently a more clearly visible plateau. Since $\eta/y = 0.0013$, the abscissa of the plateau occurs for r/y in the inertial range, at $r/y \sim 0.03$, at a smaller r/y than for the DNS data. As Re increases, η/y gets smaller and the plateau shifts to smaller values of r/y . The ordinate of the plateau is close to the predicted constant and the atmospheric results of Kurien and Sreenivasan [17] lie within the error bars for close to one decade of displacements r . Turbulent boundary layer data analyzed by Baidya and co-workers [11,18] at $y^+ = 890$ shows a plateau also over approximately one decade, whereas similar measurements at $y^+ = 330$ show only a crest instead of a plateau.

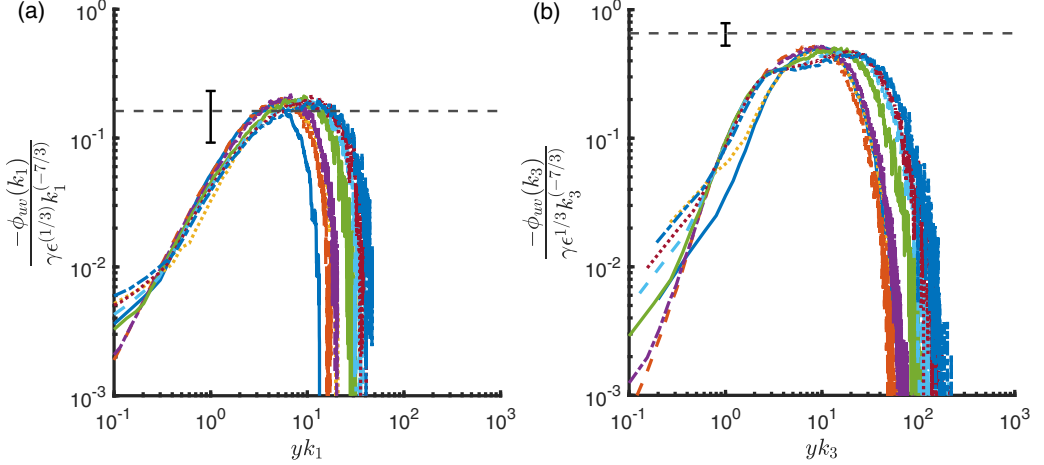


FIG. 3. (a) Compensated streamwise spectra and (b) compensated spanwise spectra for channel flow from the JHTDB. Lines have the same meanings as in Fig. 1.

Similar trends are also observed for spanwise structure functions from DNS [Fig. 2(b)], with results from the turbulent boundary layer experiments of Jacob *et al.* [9] trending towards a plateau. Nevertheless, the prefactor is notably lower than the predicted value, suggesting that in boundary layer flow, the approach to universal behavior requires even higher Reynolds numbers than those examined here. For completeness, we also compute streamwise and spanwise cospectra for the channel flow data and compare them with predictions obtained from the model of Ishihara *et al.* [12] (see Fig. 3). We normalize the cospectra by the corresponding inertial range functions defined in the preceding section [Eqs. (6) and (20)] and thus plot the compensated streamwise cospectrum $[-\phi_{uv}(k_1)/\gamma\epsilon^{1/3}k_1^{-7/3}]$ and the compensated spanwise cospectrum $[-\phi_{uv}(k_3)/\gamma\epsilon^{1/3}k_3^{-7/3}]$. We compare plateaus with the predicted inertial range behavior marked by constant ordinate lines. The spectrum at the smallest wall-normal distance $y^+ = 200$ with $Re_\tau = 1000$ possesses the smallest scale separation and therefore produces a crest around the inertial range scale. This crest broadens to a more clearly defined plateau with increasing distance from the wall, evident when compared with cospectra at $y^+ = 1500$ and $Re_\tau = 5200$. The extent of the plateau keeps increasing as the separation of scales grows with wall distance, as observed for compensated structure functions also. Comparing the scaling ranges in the cospectra to those of the mixed structure functions, it appears that power-law scaling is better for the cospectra than for structure functions.

A further observation can be made when focusing on the high-wave-number region approaching the viscous dissipation range. In Fig. 4 we show the compensated streamwise cospectrum plotted against wave numbers normalized now with the Kolmogorov length scale η , including the signed values of the spectra (i.e., skipping some low-magnitude values near zero in the log-log plot). We observe a zero crossing in the cospectra at the start of the dissipation range at a wave number $k_1 \sim 0.1/\eta$ for all cases. Since the cospectra are normalized by a positive decreasing function, high-wave-number contributions are amplified and we are able to clearly see a zero crossing, which would usually be obscured by the small magnitudes of the spectra there. This result indicates that the anticorrelation between the streamwise and wall-normal components of velocity that dominates across the energy containing length scales and the inertial range scales does not extend to motions close to the scale of the crossing. The coherent motions which cause the anticorrelation have length scales larger than $\sim 10\eta$; at smaller scales, small flow structures which result in a positive correlation occur.

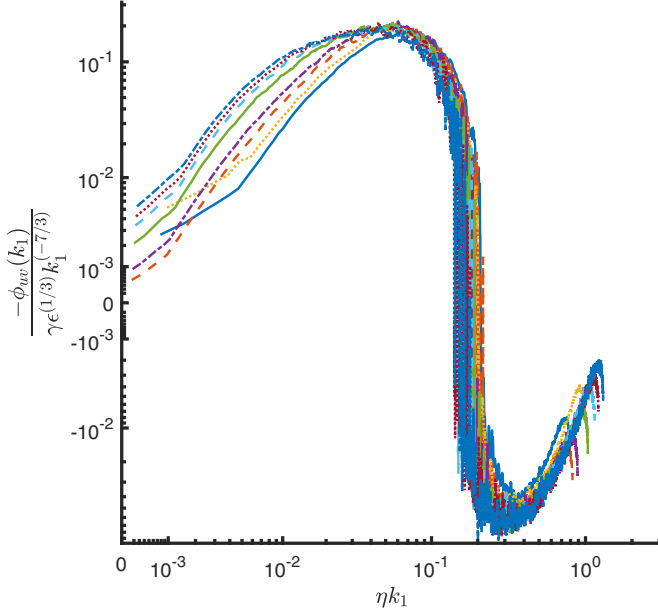


FIG. 4. Streamwise cospectra for channel flow data from the JHTDB show zero crossing at wave number $k_1 \sim 0.1/\eta$ for all cases. Lines have the same meanings as in Fig. 1.

V. CONCLUSION

A model for the inertial-range second-order structure function tensor was developed under the purview of Kolmogorov's 1941 theory, incorporating the effects of anisotropy as a linear perturbation along the lines of a spectral model developed by Ishihara *et al.* [12] and using model constants calculated for constant shear flows. This approach allows us to fully determine the structure function tensor, against which measurements from simulations and experiments can be compared. We compared two components of the structure function with the strongest dependence on the anisotropy with data from channel-flow simulations and experimental measurements. The comparisons were carried out by plotting the so-called compensated streamwise and spanwise structure functions. Good agreement was observed for the streamwise structure function. For the spanwise structure function, the magnitude from the data was lower than that predicted by the model. The difference may be associated with the fact that we considered a wall-bounded flow that differs from homogeneous free shear flow by the blocking effects of the wall. Since the dominant streamwise-aligned vortical flow structures have similar scales in the vertical and spanwise directions, we speculate that the spanwise two-point statistics are also affected by the presence of the wall while the streamwise direction remains less affected. Additionally, spanwise and streamwise cospectra were also compared with modeled behavior and good agreement was found. We also reported a zero crossing in the streamwise cospectra, occurring at a length scale close to the dissipation scale. This result suggests that small-scale motions behave opposite to the behavior of large-scale motions since they cause positive correlation of streamwise and wall-normal components of the velocity that dominates at very small scales.

ACKNOWLEDGMENTS

We are grateful to the National Science Foundation (Grant No. CBET 1738918) and the Simons Foundation (Targeted Grant No. MPS-663054) for financial support. Data were obtained from the turbulence database system supported by the National Science Foundation Grant No. CSSI-210387.

- [1] S. B. Pope, *Turbulent Flows* (Cambridge University Press, Cambridge, 2000).
- [2] U. Frisch, *Turbulence: The Legacy of A. N. Kolmogorov* (Cambridge University Press, Cambridge, 1995).
- [3] S. G. Saddoughi and S. V. Veeravalli, Local isotropy in turbulent boundary layers at high Reynolds number, *J. Fluid Mech.* **268**, 333 (1994).
- [4] J. L. Lumley, Similarity and the turbulent energy spectrum, *Phys. Fluids* **10**, 855 (1967).
- [5] P. A. Davidson, T. B. Nickels, and P.-Å. Krogstad, The logarithmic structure function law in wall-layer turbulence, *J. Fluid Mech.* **550**, 51 (2006).
- [6] I. Arad, B. Dhruba, S. Kurien, V. S. L'vov, I. Procaccia, and K. R. Sreenivasan, Extraction of Anisotropic Contributions in Turbulent Flows, *Phys. Rev. Lett.* **81**, 5330 (1998).
- [7] I. Arad, V. S. L'vov, and I. Procaccia, Correlation functions in isotropic and anisotropic turbulence: The role of the symmetry group, *Phys. Rev. E* **59**, 6753 (1999).
- [8] L. Biferale and I. Procaccia, Anisotropy in turbulent flows and in turbulent transport, *Phys. Rep.* **414**, 43 (2005).
- [9] B. Jacob, C. M. Casciola, A. Talamelli, and P. H. Alfredsson, Scaling of mixed structure functions in turbulent boundary layers, *Phys. Fluids* **20**, 045101 (2008).
- [10] C. M. de Silva, I. Marusic, J. D. Woodcock, and C. Meneveau, Scaling of second- and higher-order structure functions in turbulent boundary layers, *J. Fluid Mech.* **769**, 654 (2015).
- [11] X. I. A. Yang, R. Baidya, P. Johnson, I. Marusic, and C. Meneveau, Structure function tensor scaling in the logarithmic region derived from the attached eddy model of wall-bounded turbulent flows, *Phys. Rev. Fluids* **2**, 064602 (2017).
- [12] T. Ishihara, K. Yoshida, and Y. Kaneda, Anisotropic Velocity Correlation Spectrum at Small Scales in a Homogeneous Turbulent Shear Flow, *Phys. Rev. Lett.* **88**, 154501 (2002).
- [13] Y. Kaneda, Linear response theory of turbulence, *J. Stat. Mech.: Theor. Exp.* (2020) 034006.
- [14] Y. Li, E. Perlman, M. Wan, Y. Yang, C. Meneveau, R. Burns, S. Chen, A. Szalay, and G. Eyink, A public turbulence database cluster and applications to study Lagrangian evolution of velocity increments in turbulence, *J. Turbul.* **9**, N31 (2008).
- [15] J. Graham, K. Kanov, X. I. A. Yang, M. Lee, N. Malaya, C. C. Lalescu, R. Burns, G. Eyink, A. Szalay, R. D. Moser, and C. Meneveau, A web services accessible database of turbulent channel flow and its use for testing a new integral wall model for LES, *J. Turbul.* **17**, 181 (2016).
- [16] M. Lee and R. D. Moser, Direct numerical simulation of turbulent channel flow up to $Re_\tau \approx 5200$, *J. Fluid Mech.* **774**, 395 (2015).
- [17] S. Kurien and K. R. Sreenivasan, Anisotropic scaling contributions to high-order structure functions in high-Reynolds-number turbulence, *Phys. Rev. E* **62**, 2206 (2000).
- [18] K. M. Talluru, R. Baidya, N. Hutchins, and I. Marusic, Amplitude modulation of all three velocity components in turbulent boundary layers, *J. Fluid Mech.* **746**, R1 (2014).
- [19] S. Kurien, V. S. L'vov, I. Procaccia, and K. R. Sreenivasan, Scaling structure of the velocity statistics in atmospheric boundary layers, *Phys. Rev. E* **61**, 407 (2000).
- [20] A. N. Kolmogorov, Dissipation of energy in the locally isotropic turbulence, *Dokl. Akad. Nauk SSSR* **32**, 16 (1941).
- [21] A. N. Kolmogorov, The local structure of turbulence in incompressible viscous fluid for very large Reynolds numbers, *Dokl. Acad. Nauk SSSR* **30**, 301 (1941).
- [22] B. J. Rosenberg, M. Hultmark, M. Vallikivi, S. C. C. Bailey, and A. J. Smits, Turbulence spectra in smooth- and rough-wall pipe flow at extreme Reynolds numbers, *J. Fluid Mech.* **731**, 46 (2013).
- [23] S. Bonetti, G. Manoli, C. Manes, A. Porporato, and G. G. Katul, Manning's formula and Strickler's scaling explained by a co-spectral budget model, *J. Fluid Mech.* **812**, 1189 (2017).
- [24] J. H. Silverman, Taxicabs and sums of two cubes, *Am. Math. Mon.* **100**, 331 (1993).
- [25] <http://turbulence.pha.jhu.edu/datasets.aspx>